Mathematical Geology, Vol. 36, No. 1, January 2004 (© 2004)

Applicability of a Backprojection Algorithm to Reconstruct Images of Subsurface Horizontal Planes for Laboratory Experiments in Electrical Resistance Tomography[1]

Josep Jordana[2] and Ramon Pallàs-Areny[2]

This paper describes the use of a backprojection algorithm to reconstruct subsurface images of the electrical resistivity in horizontal planes parallel to the surface. The algorithm can be applied to detect buried objects such as tanks or pipes and possible leakages from them. Two imaging strategies are compared: juxtaposition of vertical planes, and 3D reconstruction from the sensitivity matrix corresponding to the entire volume whose surface is explored. The electrode arrays used for voltage measurement are the dipole–dipole array and a modified Schlumberger array. A personal computer controls current injection, electrode switching, and voltage detection. The system injects 1 kHz, 20 V peak-to-peak square waveforms, thus avoiding electrode polarization effects. Experimental laboratory measurements show that the algorithm detects localized objects such as an insulating sphere and a conductive cylinder immersed in water. Furthermore, covering half of the cylinder by a rubber sleeve to simulate a nonconductive leak, yields a distinct image for the leak. The backprojection algorithm does not need any regularization parameter and it is very fast in inverting the sensitivity matrix because it approximates the inverse matrix by its transposed. The dipole–dipole array usually yields a lower overall pixel error than the modified Schlumberger array but both allow the detection of simulated underground leaks.

KEY WORDS: electrode array, sensitivity theorem, geoelectrics, leak detection.

INTRODUCTION

Electrical resistance tomography (ERT) aims to image the distribution of resistivity or conductivity across a section of a body from boundary voltage measurements when injecting current. ERT was first proposed in geophysics (Dines and Lytle, 1981), and it has also found industrial and medical applications. Geoelectrical prospecting methods have been available for more than a century, for example to

[1]Received 18 August 2002; accepted 25 August 2003.

[2]Dept. d'Enginyeria Electrònica, Universitat Politècnica de Catalunya, Escola Politècnica Superior de Castelldefels, Avda del Canal Olímpic s/n, 08860 Castelldefels, Barcelona, Spain; e-mail: jordana@eel.upc.es

0882-8121/04/0100-0127/1 © 2004 International Association for Mathematical Geology

detect subsurface objects from electrical resistivity variations inferred from surface voltage measurements. These methods are common in shallow subsurface investigations, especially for groundwater studies (Burger, 1992). Currently, there is a variety 2D and 3D algorithms able to image underground resistivity distributions. Several of those algorithms derive from ERT for medical applications (Barber, 1990; Kotre, 1993). Subsurface resistivity imaging has been proposed, for example, for leak detection because it is less expensive than methods based on soil sampling and borehole tomography (Jordana, Gasulla, and Pallàs-Areny, 2001). Specifically, subsurface resistivity measurements to detect leaks from buried pipes do not need soil drilling.

Many underground resistivity imaging techniques use least-squares-based methods. But inverse geoelectrical problems are ill-conditioned in general, meaning that the images obtained are very sensitive to measurement errors. This paper analyzes a weighted backprojection algorithm, based on the sensitivity theorem, whose details have been reviewed by Wang (2002).

In a previous work (Jordana, Gasulla, and Pallàs-Areny, 2001), we used a linear electrode array to image the resistivity distribution across the vertical plane containing the array. The best images were obtained when the array was on the same plane as the object to detect, whose location is often difficult to know in advance. Here we propose to explore a region by uniformly shifting a single linear array of N electrodes to N_s successive parallel positions (Fig. 1). This method allows us to image resistivity distributions in horizontal planes parallel to the surface at different depths. The system has been successfully tested in a phantom with tap water and different spherical and cylindrical objects immersed.

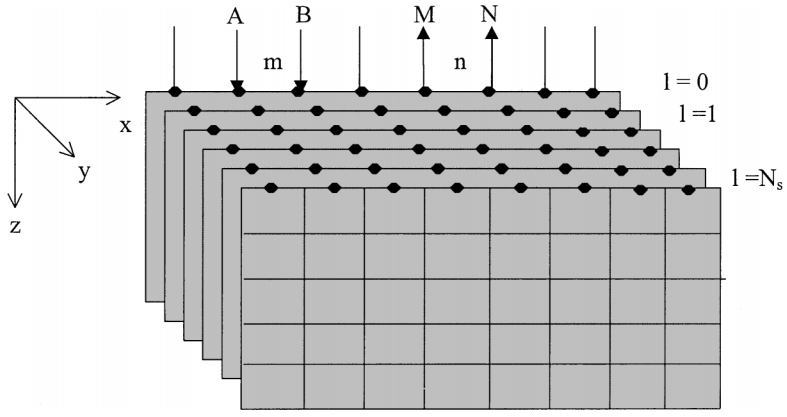

Figure 1. Shifting a linear array of N electrodes to N_s parallel positions allows us to image horizontal planes by juxtaposing the N_s 2D images corresponding to vertical planes. Shifting two orthogonal electrode arrays allows us to directly obtain 3D images.

IMAGE RECONSTRUCTION ALGORITHM

The image-reconstruction algorithm here proposed is based on the sensitivity theorem (Geselowitz, 1971). The algorithm relies on the following assumptions:

(i) The measured data are the real part of the impedance. Hence, images correspond to underground conductivity or resistivity distributions.
(ii) The interelectrode separation (s) is uniform.
(iii) The background conductivity distribution is homogeneous (σ_h).
(iv) The changes in conductivity to be imaged are not very different from the homogeneous distribution.
(v) For so-called 2D algorithms, the region to be imaged is considered bidimensional, that is, neither vertical planes nor horizontal planes interact.

In spite of (iv), Experimental Results and Discussion section show that tests performed with objects whose conductivity is very different from that of the surrounding medium yield useful images because the algorithms are intended to detect changes in conductivity rather than to quantify them.

Data for underground resistivity imaging are collected from a surface linear array of uniformly spaced electrodes (electrode spacing s), alternately used for both current injection and voltage detection. Here we use the dipole–dipole and the so-called modified Schlumberger electrode arrays (Fig. 2). For a given set of N electrodes, the respective number of independent measurements are $N(N-3)/2$ for the dipole–dipole array and $(N-2)(N-3)/2$ for the modified Schlumberger array. The modified Schlumberger array yields a reduced number of measurements but the measured voltages are higher than those of the dipole–dipole array.

Figure 1 shows the volume explored by shifting the linear array. This method has the advantage of allowing the exploration of horizontal planes, which should better identify underground objects or anomalies. Furthermore, because we assume that vertical planes are independent from each other, the sensitivity matrix (Kotre, 1996) is the same for each position of the electrode array. Therefore, we only need N_s reconstructions, N_s being the number of positions of the electrode array: the sensitivity matrix corresponding to each array position will be the same as that for 2D vertical planes. The juxtaposition of images of successive vertical planes yields more information than the image of a single vertical plane and permits us to reconstruct horizontal planes. If the distance between successive array positions equals s (interelectrode spacing), the reconstructed horizontal planes are squares.

When using an array of eight electrodes, the order of the sensitivity matrix is 20×40 for the dipole–dipole array and 15×40 for the modified Schlumberger array. The number of rows corresponds to the number of independent measurements and the number of columns corresponds to the number of pixels to reconstruct. If

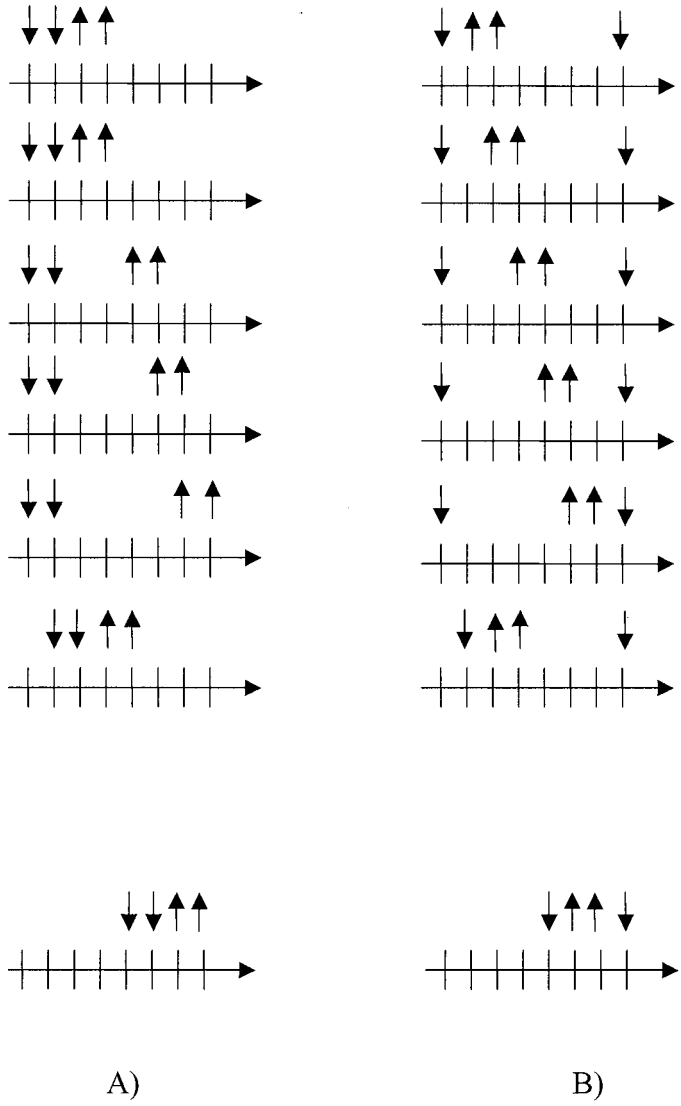

Figure 2. Electrode arrays description: (A) In the dipole–dipole array, current injection and voltage detection are performed by adjacent electrode pairs, including end electrodes. (B) In the modified Schlumberger array, current is injected through distant electrodes and voltage is detected by successive adjacent electrode pairs.

the array is shifted seven times (eight positions), we need to invert the sensitivity matrix eight times.

In practice, because electrical charge flows throughout the underground, voltages sensed by electrodes depend not only on the vertical plane beneath the electrode array but also on nearby vertical planes. In order to take this effect into account, we calculate the sensitivity coefficients for the complete volume and apply them to the reconstruction of 3D images from data obtained by two orthogonal electrode arrays, as proposed by Kotre (1996). When using two eight-electrode arrays, the order of the sensitivity matrix is 320×320 for the dipole–dipole array and 240×320 for the modified Schlumberger array.

The backprojection image-reconstruction algorithm has been applied to obtain 2D images from vertical planes that are later juxtaposed, and 3D images that are reconstructed from measurements obtained by shifting two orthogonal linear electrode arrays.

When the resistivity changes, the change in voltage corresponding to an injecting–detecting electrode pair m–n as a function of the sensitivity coefficients obeys to

$$\left(\frac{V - V_{\mathrm{h}}}{V_{\mathrm{h}}}\right)_{m,n} = \frac{\sum_x \sum_y \sum_z S_{m,n,x,y,z} \left(\frac{\rho - \rho_{\mathrm{h}}}{\rho_{\mathrm{h}}}\right)_{(x,y,z)}}{\sum_x \sum_y \sum_z S_{m,n,x,y,z}} \tag{1}$$

where V are the measured voltages when there is the anomaly, V_{h} are the measured voltages for an homogeneous medium, and $S_{m,n,x,y,z}$ is the sensitivity coefficient relating the measurement (m, n) to the position (x, y, z). The sensitivity coefficients are calculated in the appendix. For several injecting–detecting pairs, (1) leads to an equation system relating small conductivity changes to voltage changes measured on the surface. The normalized resistivity is then (Kotre, 1996)

$$P(x, y, z) = \frac{\sum_m \sum_n S_{m,n,x,y,z} \left(\frac{V - V_{\mathrm{h}}}{V_{\mathrm{h}}}\right)_{(m,n)}}{\sum_m \sum_n S_{m,n,x,y,z}} \tag{2}$$

This reconstruction method approximates the inverse sensitivity matrix by its transposed, whose values (reconstructed pixels) are

$$P(x, y, z) \approx -\frac{\sigma(x, y, z) - \sigma_{\mathrm{h}}}{\sigma_{\mathrm{h}}} \tag{3}$$

where σ_{h} is the reference conductivity (homogeneous medium) and $\sigma(x, y, z)$ is the true conductivity distribution, slightly different from the homogeneous distribution. Some experimental measurements later described actually involve high-contrast objects, but the algorithm detects them too.

This reconstruction algorithm yields blurred images that can be restored by a spatial frequency filter derived from the algorithm's *point-spread-function* (PSF). Leak detection, however, only needs to distinguish between images showing an intact pipe and images showing a leaking pipe. There is no need for neat images, and experimental results without any restoration filter are acceptable.

EXPERIMENTAL RESULTS AND DISCUSSION

The proposed algorithm has been applied to reconstruct images from data obtained from a 40 cm $\times$ 30 cm $\times$ 25 cm plastic tank full of tap water, where we have explored a 16 cm $\times$ 16 cm area. The instrumentation electronics for current injection and voltage detection has been described elsewhere (Gasulla, Jordana, and Pallàs-Areny, 1998). A personal computer controls electrode switching, thus enabling us to easily test different electrode arrays. The system injects 1 kHz, 20 V peak-to-peak square waveforms, thus avoiding electrode polarization effects, which hinder dc and low-frequency voltage measurements.

Figure 3 is a sketch of the tank as viewed from its top. The plane to be reconstructed is divided in 8 $\times$ 8 pixels. The electrode arrays can be respectively displaced along the x and the y directions. Actual electrode spacing is $s = 2$ cm. In order to obtain conclusions independent of specific distances, all the other distances and dimensions are given in terms of s. The objects that we have immersed in the tank are: (a) an insulating sphere of radius 1 s buried at 2 s (4 cm) and (b) a stainless steel cylinder of radius 1 s and length 8 s also buried at 2 s and parallel to

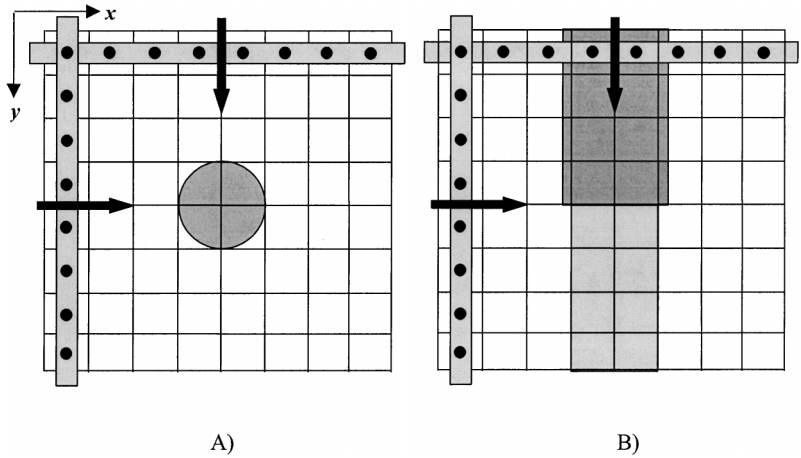

Figure 3. Orthogonal electrode arrays in a plastic tank full of tap water, view from above when immersing: (A) an insulating sphere and (B) a conductive cylinder half of which is covered by an insulating sleeve to simulate a leak.

the y axis. Half of the cylinder was covered by an insulating rubber sleeve 0.25 s (0.5 cm) thick to simulate an insulating leak from the cylinder.

Displacing the electrode arrays at uniform steps can only be approximated in practice. Electrode spacing in a fixed 8×8 electrode matrix would be easier to control, but at a higher cost for the electrode switching system.

Particularities of visual perception in humans make the quality of the reconstructed images dependent on the color map used to picture them (Rogowitz and Treinish, 1998). Hence, equal pixel values can result in quite different images perceived. Therefore, instead of relying on visual perception only, we have also compared the reconstructed images by calculating the root-mean-square error between ideal and actual pixel values,

$$E = \frac{1}{P} \sum_{n=1}^{P} e_i^2 \tag{4}$$

$$e_i = \frac{\sigma_i^{\text{ideal}}}{\left|\sigma_{i_{\max}}^{\text{ideal}}\right|} - \frac{\sigma_i^r}{\left|\sigma_{i_{\max}}^r\right|} \tag{5}$$

where P is the number of pixels in the image, and σ_i^{ideal} and $|\sigma_{i_{\max}}^{\text{ideal}}|$, and σ_i^r and $|\sigma_{i_{\max}}^r|$ are, respectively, the values of pixel i and the maximal absolute values of pixels in the ideal and reconstructed images. Both ideal and reconstructed pixel values are normalized to their respective maximal values in order to better compare the ideal and reconstructed images. E is the overall pixel error.

Image Reconstruction for an Insulating Sphere

Figure 4 shows the theoretical image corresponding to an insulating sphere of radius 1 s immersed at depth 2 s. We see a square instead of a circle because of the large pixel size. The negative values for the conductivity of the central area (shown in black) indicate that the object is insulating as compared to its surroundings.

Results With the Dipole–Dipole Array

Figure 5(A) shows the image for the horizontal plane at $z = 2$ s obtained by juxtaposition of vertical planes (parallel to axis y) reconstructed by the back-projection algorithm applied to data from the dipole–dipole array. The insulating sphere can be easily identified. Figure 5(B) shows the image of the same horizontal plane obtained from data also gathered with the dipole–dipole array but by shifting the orthogonal electrode array and image reconstruction based on the sensitivity matrix corresponding to the whole volume shown in Figure 1, whose order is

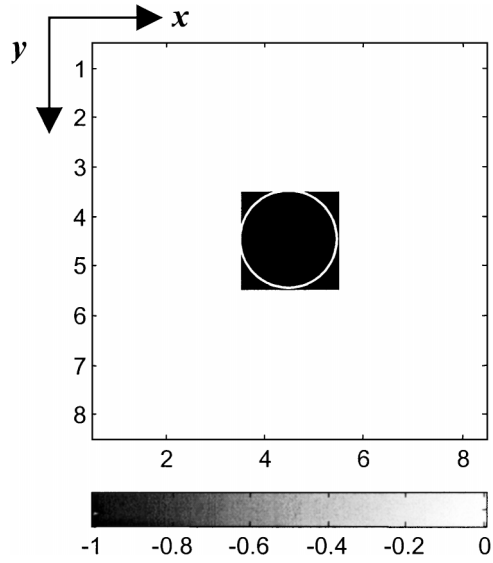

Figure 4. Ideal image of a sphere of radius 1 *s* (*s* being the electrode spacing), and placed at 2 *s* depth. The sphere occupies the four central pixels of its plane.

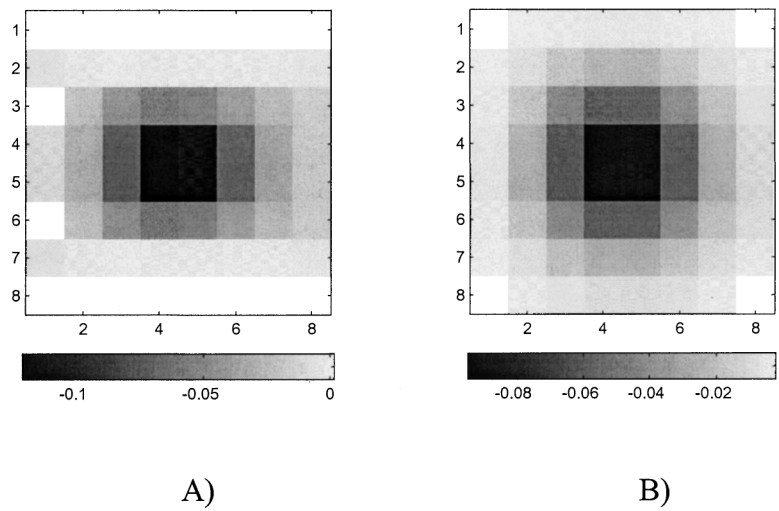

Figure 5. Reconstructed image for the sphere in Figure 3(A) when buried at 2 *s* depth, when using the backprojection method and the dipole–dipole array (interelectrode distance 1 *s*). (A) Image synthesized by juxtaposing vertical planes. (B) 3D image obtained from voltages measured by shifting two linear orthogonal arrays.

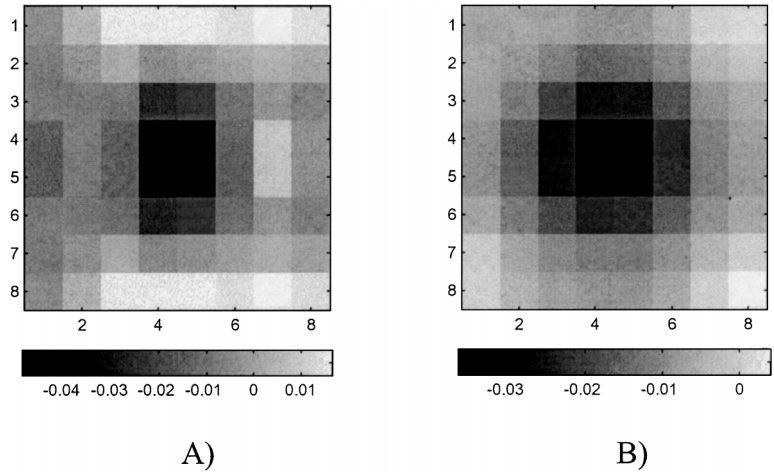

Figure 6. Reconstructed image for the sphere in Figure 3(A) when buried at 2 s depth, when using the modified Schlumberger array (interelectrode distance 1 s). (A) Image synthesized by juxtaposing vertical planes. (B) 3D image obtained from voltages measured by shifting two linear orthogonal arrays.

320×320 in this case. The sphere is easily identified but $E = 0.080$, against $E = 0.054$ in Figure 5(A). This increase in error can be partially attributed to nonuniform steps when shifting the electrode arrays.

Results With the Modified Schlumberger Array

Figure 6 shows images reconstructed by applying the backprojection algorithm to voltages measured by the modified Schlumberger array. The sphere can still be identified but the images are clearly worse than those in Figure 5. However, $E = 0.049$ and $E = 0.108$, respectively for Figure 6(A) and (B). This indicates that perhaps the overall pixel error E is not the best parameter to quantify image quality. An error metric linked only to those pixels of interest could be more meaningful.

Image Reconstruction for a Conducting Cylinder With a Simulated Insulating Leak

Figure 7 shows the theoretical image of the conducting cylinder with a simulated insulating leak, placed at the horizontal plane $z = 2\,s$. Results in the previous section for the sphere indicate that using the 3D sensitivity matrix for voltage data measured by displacing the orthogonal array does not improve enough the

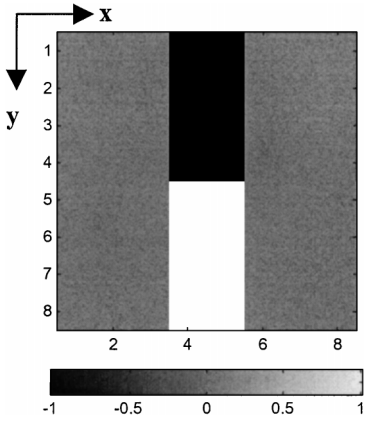

Figure 7. Ideal image of the horizontal plane at $z = 2\ s$ for a conductive cylinder with radius $1\ s$ and length $8\ s$, with a simulated insulating leak whose thickness is $0.25\ s$. (Pixels in black indicate the insulating leak.)

quality of images to compensate for the increased computation time required. Consequently, here we show only images obtained by juxtaposing vertical planes corresponding to successive positions of the electrode array parallel to the x axis.

Figure 8(A) and (B) shows images of the horizontal plane at $z = 2\ s$ reconstructed by, respectively, the dipole–dipole electrode array and the modified Schlumberger array. Both arrays detect the cylinder and the simulated leak, and their correct locations. The overall pixel errors are similar: $E = 0.102$ and $E = 0.132$.

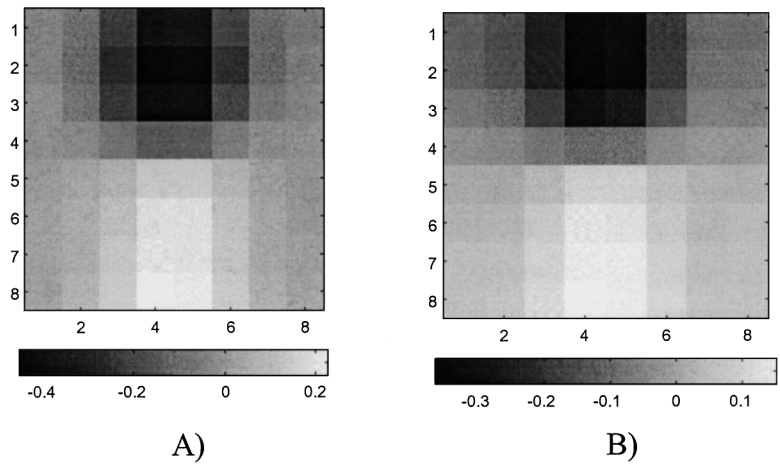

Figure 8. Reconstructed image for the cylinder in Figure 3(B) when buried at $2\ s$ depth, by juxtaposing vertical planes when using (A) the dipole–dipole array and (B) the modified Schlumberger array.

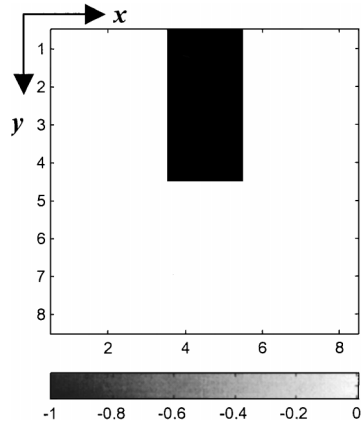

Figure 9. Ideal image for the leak in Figure 3(B) when reference voltages are measured in the presence on the intact conductive cylinder.

Image Reconstruction for a Conducting Cylinder With a Simulated Insulating Leak and In-Situ Reference Voltages

Reference voltages in the preceding sections (V_h in Eqs. (1) and (2)), were obtained by first measuring voltages in a tank without any immersed object. This is not a realistic situation for leak detection but allows the comparison of different electrode arrays. Figure 9 shows the ideal image for the simulated leak when the reference voltages correspond to an intact conductive cylinder immersed in the tank.

Figure 10(A) and (B) shows images of the horizontal plane at $z = 2$ *s* reconstructed by, respectively, the dipole–dipole electrode array and the modified Schlumberger array. Both arrays detect the cylinder and the simulated leak, and their correct locations. The overall pixel errors are similar: $E = 0.052$ and $E = 0.063$.

CONCLUSIONS

The backprojection algorithm allows the fast reconstruction of images obtained from voltages measured by the dipole–dipole and modified Schlumberger linear electrode arrays when applied to subsurface resistance tomography. As opposed to other image reconstruction algorithms, the backprojection algorithm does not need to guess any regularization parameter. Images from horizontal planes parallel to the surface can be obtained by either juxtaposing images of vertical planes containing the electrode array that is successively shifted to parallel positions, or 3D image-reconstruction algorithms applied to voltage data obtained by shifting two orthogonal linear arrays.

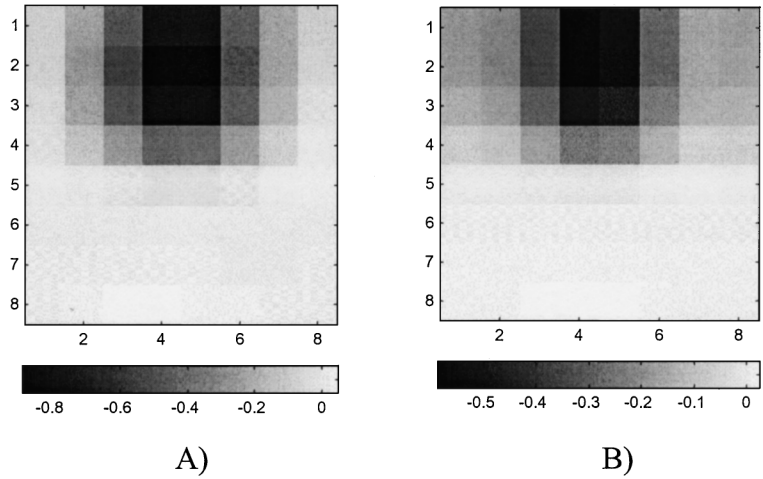

Figure 10. Reconstructed image for the simulated leak in Figure 3(B) when the cylinder is buried at 2 *s* depth and the leak is 0.25 *s* thick, by juxtaposing vertical planes when using reference voltages measured with the intact immersed cylinder, using: (A) the dipole–dipole array, (B) the modified Schlumberger array.

Experimental tests in a water-filled plastic tank with an immersed sphere or cylinder, show that the juxtaposition of vertical planes corresponding to a single electrode array shifted to successive positions, permits the detection of both the object and a simulated leak from the cylinder. 3D image reconstruction methods also permit us to detect both objects and simulated leaks, but with a higher computation time without substantial reduction in overall pixel error. This may be due to a nonuniform placement of the electrode array in successive parallel positions.

Simulated insulating leaks can be detected and correctly located when the reference voltages for image reconstruction are measured in the presence of an intact conductive cylinder, which is a situation closer to the actual than measuring reference voltages from a volume without any internal object.

The dipole–dipole electrode array usually yields images with lower overall pixel error than the modified Schlumberger array. Visually, however, both arrays yield images of comparable quality.

REFERENCES

Barber, D. C., 1990, Quantification in impedance imaging: Clin. Phys. Physiol. Meas. v. 11, p. A45–A56.

Burger, R. H., 1992, Exploration geophysics of the shallow subsurface: Prentice Hall, Englewood Cliffs, NJ, 483 p.

Dines, K. A., and Lytle, R. J., 1981, Analysis of electrical conductivity imaging: Geophysics, v. 46, p. 1025–1036.

Gasulla, M., Jordana, J., and Pallàs-Areny, R., 1998, Subsurface resistivity measurement using square waveforms: IEEE Trans. Instrum. Meas., v. 47, p. 74–77.

Geselowitz, D. B., 1971, An application of electrocardiographic lead theory to impedance plethysmography: IEEE Trans. Biomed. Eng., v. 18, p. 38–41.

Jordana, J., Gasulla, M., and Pallàs-Areny, R., 2001, Electrical resistance tomography to detect leaks from buried pipes: Meas. Sci. Technol., v. 12, p. 1061–1068.

Kotre, C. J., 1993, Studies of image reconstruction methods for electrical impedance tomography: Doctoral Dissertation, University of Newcastle-Upon-Tyne, 72 p.

Kotre, C. J., 1996, Subsurface electrical impedance imaging using orthogonal linear electrode arrays: IEE Proc. A, v. 143, p. 41–46.

Noel, M., and Xu, B., 1991, Archaeological investigation by electrical resistivity tomography: A preliminary study: Geophys. J. Int., v. 107, p. 95–102.

Rogowitz, B., and Treinish, L., 1998, Data visualization: The end of the rainbow: IEEE Spectrum, v. 35, no. 12, p. 52–59.

Wang, M., 2002, Inverse solutions for electrical impedance tomography based on congujate gradients methods: Meas. Sci. Technol., v. 13, p. 101–117.

APPENDIX

Determination of the Sensitivity Coefficients and Sensitivity Matrix

To calculate the sensitivity coefficients it is necessary to know the electric potential at each pixel in which the subsurface has been divided. We consider an infinite semispace of homogeneous resistivity ρ_h. The electrostatic potential at point P due to the electrode pair (m) with currents I and $-I$ (Fig. A1) is

$$V_p = \frac{I\rho_h}{2\pi}\left(\frac{1}{a} - \frac{1}{b}\right) \tag{A1}$$

where

$$a = \sqrt{(x - x_i)^2 + (y - y_i)^2 + (z - z_i)^2}$$

$$\text{and} \quad b = \sqrt{(x - x_d)^2 + (y - y_d)^2 + (z - z_d)^2},$$

are the distances of each electrode pair to point (x, y, z). (x_i, y_i, z_i) are the coordinates of the current-injecting electrode and (x_d, y_d, z_d) are those of the current-draining electrode.

By successively taking the derivative of (A1) with respect to x, y, and z, we obtain the electric field generated by each electrode pair (m)

$$E_m = -\nabla\phi_m = -(E_{ix}, E_{iy}, E_{iz}) \tag{A2}$$

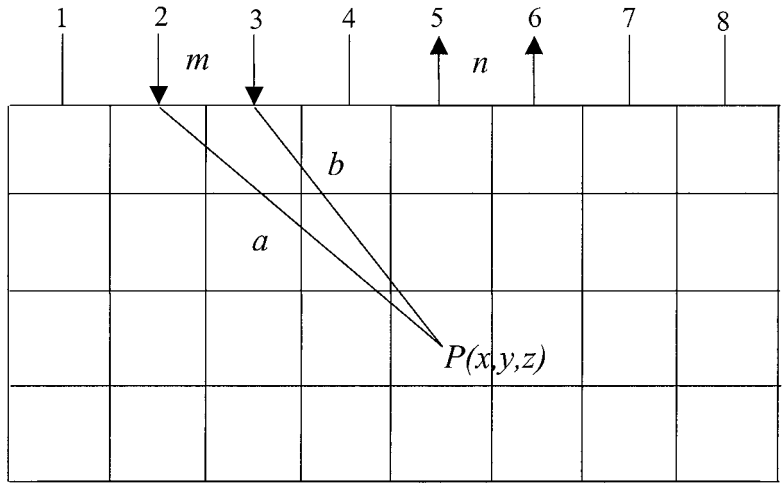

Figure A1. Notation used in determining the sensitivity coefficient of a pixel of a vertical plane under the electrode array.

The electric field components corresponding to the electrode pair m are:

$$E_{ix} = -\frac{\partial V_p}{\partial x} = k\left[\frac{x - x_i}{w_i} - \frac{x - x_d}{w_d}\right]$$
$$E_{iy} = -\frac{\partial V_p}{\partial y} = k\left[\frac{y - y_i}{w_i} - \frac{y - y_d}{w_d}\right] \qquad \text{(A3)}$$
$$E_{iz} = -\frac{\partial V_p}{\partial z} = k\left[\frac{z - z_i}{w_i} - \frac{z - z_d}{w_d}\right]$$

where

$$w_i = \left((x - x_i)^2 + (y - y_i)^2 + (z - z_i)^2\right)^{3/2},$$
$$w_d = \left((x - x_d)^2 + (y - y_d)^2 + (z - z_d)^2\right)^{3/2}$$

and $k = \frac{I\rho_h}{2\pi}$. The potential gradient corresponding to the second electrode pair (n), $\nabla\phi_n$, can be obtained in a similar way.

The sensitivity coefficients associated to each pixel equal the scalar product of the two potential gradients times its area or volume, depending on whether the reconstruction is bidimensional (2D) or tridimensional (3D). An approximate 2D sensitivity coefficient for pixel i, corresponding to the measurement j is

(Noel and Xu, 1991)

$$S_{ji} = \nabla\phi_m \nabla\phi_n A_i \tag{A4}$$

where we have supposed that its value is constant in the whole area of the element (x, y, z).

The sensitivity matrix consists of the sensitivity coefficients corresponding to a homogeneous medium. Its order is $M \times P$, where M is the number of measurements and P is the number of pixels in which the subsurface has been divided.